# Experimental Study of the Hydraulic Operation of an Annular Centrifugal Contactor with Various Mixing Vane Geometries

**Kent E. Wardle, Todd R. Allen, and Mark H. Anderson**
University of Wisconsin-Madison, Dept. of Engineering Physics, 1500 Engineering Drive, Madison, WI 53706

**Ross E. Swaney**
University of Wisconsin-Madison, Dept. of Chemical and Biological Engineering, 1415 Engineering Drive, Madison, WI 53706

*DOI 10.1002/aic.12110*
*Published online December 14, 2009 in Wiley InterScience (www.interscience.wiley.com).*

*The annular centrifugal contactor is a combination mixer/centrifuge that has been developed for solvent extraction processes for recycling used nuclear reactor fuel. The experimental observations presented were part of a simulation-focused research effort aimed at providing a more complete understanding of the fluid flow within these contactors to enable further advancements in design and operation of future units and greater confidence for use of such contactors in a variety of other solvent extraction applications. Laser doppler velocimetry (LDV), particle image velocimetry (PIV), pressure measurements, and high-speed video imaging for a range of flow rates and rotor speeds were performed to characterize the flow of water in the annular mixing region of the contactor using three different mixing vane geometries. It was found that the geometry of the mixing vanes has a significant impact on the annular liquid height and general flow in the contactor mixing zone.* © 2009 American Institute of Chemical Engineers *AIChE J,* 56: 1960–1974, 2010

*Keywords: mixing, multi-phase flow, turbulence, extraction, nuclear engineering*

## Introduction

Solvent extraction (or liquid-liquid extraction) is a process by which immiscible fluids are mixed and, subsequently, separated to achieve extraction of a desired dissolved species from one phase to the other. Such processes are employed in a variety of chemical and biological fields. Solvent extraction is also the primary process by which uranium and other elements are extracted from used nuclear fuel for partitioning or recycling. Whereas a variety of process equipment has been used historically,[1] on account of its small size and high efficiency the centrifugal contactor is the central piece of equipment for advanced processes being developed for a future used fuel processing facility.[2]

The initial design of the annular centrifugal contactor was done at Argonne National Laboratory by modification of a Savannah River Laboratory (SRL) contactor.[3,4] A sketch of a general Argonne contactor is shown in Figure 1. Contactors are typically referred to by the diameter of the rotor. Hence, a 5 cm contactor is an annular centrifugal contactor with a 5 cm dia. rotor. The annular centrifugal contactor is able to combine both the mixing and separation functions of solvent extraction in a single compact device. Flows of immiscible liquids enter through tangential ports into the annular mixing region, where the dispersion begins to form as the fluids are mixed by shear induced by the spinning rotor. Radially oriented vanes below the rotor break the rotation of the dispersion and force the liquid into the hollow rotor

Correspondence concerning this article should be addressed to K. E. Wardle at Wardle at kwardle@anl.gov.

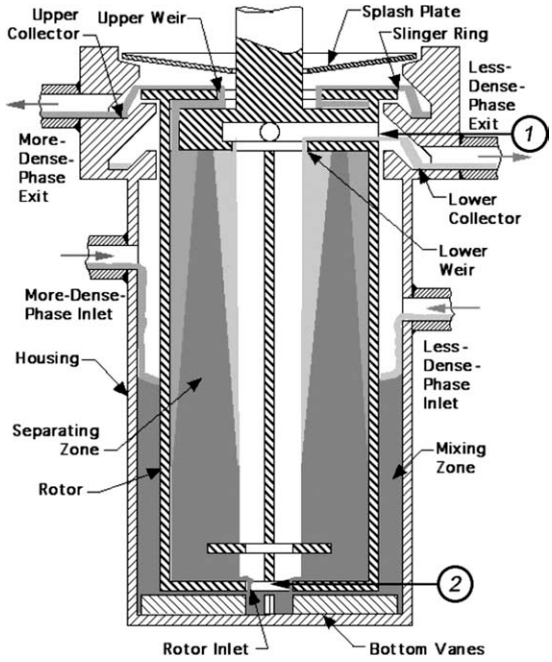


**Figure 1. Sketch of the cross-section of an annular centrifugal contactor with the main components labeled.**

Figure modified from Leonard et al. 2002.[6]

which then acts as a centrifuge separating the two phases and pumping the liquid upward. The separated phases then flow over their respective weirs and out the exit lines, flowing by gravity to successive stages or collection vessels. In this way the contactor acts as a mixer, a centrifuge, and a pump. Contactors can be set up in a linear bank of multiple units with countercurrent flow requiring no interstage pumps. The design is necessarily simple (with only a single moving part—the rotor) in order to enable the remote operation and maintenance necessary for processing used nuclear fuel.

Various experimental studies using centrifugal contactors have noted the effect of mixing vane geometry on the flow in the annular region and the resulting extraction efficiencies. Birdwell and Anderson[5] compared the extraction efficiency of 5 cm contactor operated with eight straight vanes vs. eight curved vanes and found that for low-flow rates, the curved vane geometry exhibited poorer extraction efficiency. This result was attributed to an inadequate annular liquid height for the curved vane geometry. However, Leonard et al.[6] reported annular liquid heights (ALH) as measured above the rotor bottom for three different vane geometries (four straight vanes, eight straight vanes, eight curved vanes), and observed that the eight straight vane geometry had a low-liquid level over a very wide range of flow rates, and that the curved vanes appeared to generally have a higher liquid height than the eight straight vanes. Other studies have also observed poor operation at low-flow rates.[7] Beyond these various observations, there has not been a detailed comparative flow analysis of different vane geometries prior to this current work.

The experimental observations reported here were part of a simulation-focused research effort[8] aimed at providing a more complete understanding of the fluid flow within these contactors to enable advancements in design and operation of future units, and greater confidence for use of such contactors in a variety of other solvent extraction applications. Experimental observations using a variety of techniques were performed to provide data for comparison with simulations at specific conditions (600 mL/min and 3,600 RPM) as reported in Wardle et al. 2008.[9] The simulations were found to be very consistent with the experimental observations. This article presents additional experimental measurements that were performed as part of the overall effort to explore the hydraulic operation of the contactor over a range of operational conditions (i.e., flow rates and rotor speeds). The flow in rotating annular domains is typically characterized by the Taylor number (Ta), which is a ratio of the centrifugal forces to the viscous forces and can be defined according to Eq. 1 where $\Delta r$ is width of the annular gap between the housing radius $r_h$ and the rotor radius $r_r$ ($\Delta r = r_h - r_r$), $\Omega$ is the rotational speed, and $v$ the kinematic viscosity.

$$\mathrm{Ta} = \frac{r_r(\Delta r)^3\Omega^2}{v^2} \tag{1}$$

$$\mathrm{Re} = \frac{(r_r\Omega)\Delta r}{v} \tag{2}$$

Equation 1 is equivalent to $\mathrm{Ta} = \mathrm{Re}^2(1-\eta)/\eta$ where the Reynolds number (Re) is defined by Eq. 2 and $\eta$ is the radius ratio. Depending on the Reynolds number (or Taylor number) of the flow there can exist different characteristic flow regimes for traditional Taylor-Couette flow in single-phase systems.[10] Absent the free surface, all of the rotation speeds explored here are well into the turbulent Taylor vortex regime with $\mathrm{Ta} > 6.2 \times 10^8$ and $\mathrm{Re} > 5 \times 10^4$.

## Experimental Methods

### *Modified CINC V-2 centrifugal contactor*

The experiments were done using a centrifugal contactor manufactured by CINC Industries, which was originally purchased by Argonne National Laboratory with a nonstandard, transparent acrylic contactor housing with tangential inlets as described by Leonard et al.[6] This contactor has a rotor radius $r_r$ of 2.54 cm, and a housing radius $r_h$ of 3.17 cm, resulting in an annular gap of 0.63 cm, and a radius ratio $r_r/r_h$ of 0.8. To make detailed optical measurements possible, this same contactor unit was further modified such that the lower portion of the housing was replaced with a polished quartz cylinder. A small, triangular quartz window was also placed in the bottom vane plate to allow visualization/measurement of the flow beneath the rotor. The modified contactor is shown in Figure 2. The bottom portion of the rotor, the vane plate, and the bottom support plate were painted black in order to reduce reflections. The 8-vane plate is shown in place in Figure 2, and the other two vane plates are shown in Figure 3. The 8-vane and 4-vane plates were constructed of polyvinylidene fluoride (PVDF) and both were modified with a triangular quartz window (the 4-vane plate is shown in Figure 3a). The V-2 unit as manufactured by CINC comes standard

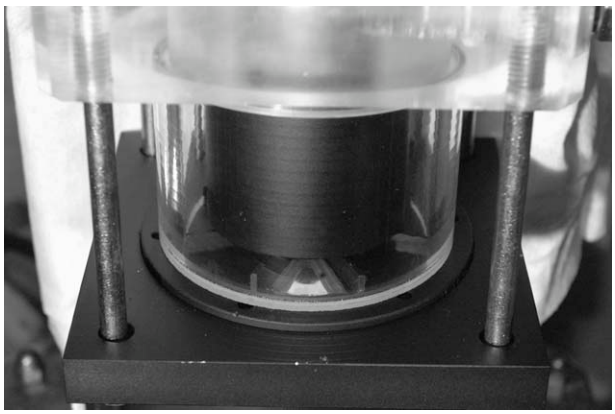

**Figure 2. Modified contactor housing with reflective parts painted black.**

The quartz cylinder shown here was a backup one that had not been polished and shows visible striations from manufacturing. The actual cylinder was ground and polished to approximately a 5 $\mu$m surface roughness.

with a stainless steel curved-vane plate. This plate was also painted and used for selected observations, but did not have a window (Figure 3b), and, thus, was not used for PIV measurements.

Since the contactor was used only for hydraulic operation with distilled water as the working fluid, the flow system was set up for continuous recirculation as shown in Figure 4. No attempt was made to actively de-gas the feed liquid; however, inlet flow tubes extended to the base of the feed/receiving container and outlet streams were run down the container wall to avoid splashing and air intake at the pumps. The pumps were positive displacement piston pumps manufactured by Fluid Metering Incorporated (FMI). One pump had a 0.635 cm (0.25 in) piston, and the other had a 0.3175 cm (0.125 in) piston. Calibration curves were generated for each of the pumps. In practice, however, the flow rate was physically measured by timed flow from the heavy phase exit line into a volumetric cylinder for each set of measurements.

### *Pressure measurements*

As shown in Figure 1, the centrifugal contactor consists of two main regions, the annular mixing region (including the vane region under the rotor) and the separation region within the rotor. From a modeling perspective, it was useful to subdivide the contactor into two separate models (simulations of the mixing zone[9] and separation zone[11] are reported separately). However, it is critical to understand how the two regions communicate in the real system in order to select an accurate representation of the boundary conditions. This is particularly true for the exit of the mixing zone (rotor inlet) for which an accurate representation of the pressure must be specified to correctly predict the volume of liquid maintained in the mixing zone. With this primary purpose, measurements of the static pressure at the rotor inlet were performed.

A Siemans differential pressure transducer (model PN-32) with a range of 1−20 mbar and an accuracy of $\pm 1$ Pa was used for these measurements. One side of the transducer was open to the atmosphere, and the other side was connected to a 1.59 mm (1/16″) OD stainless steel tube which was inserted into the drain connection of the contactor located along the rotor axis as shown in Figure 5. The probe tube was filled with water, and, therefore, it was necessary to determine the "zero" relative pressure reading once the probe was positioned. In order to minimize the static head in the tube (and maximize the measurement range), the transducer was elevated such that its position was only slightly lower than the top of the probe. The "zero" pressure reading was determined by taking the average of multiple measurements of the static liquid height of water above the probe end. Typical standard deviations for these calibration measurements were approximately $\pm 3$ Pa; this is a measure of the absolute offset of a given set of measurements and can be taken as the overall accuracy of the pressure measurements, although the relative error between different

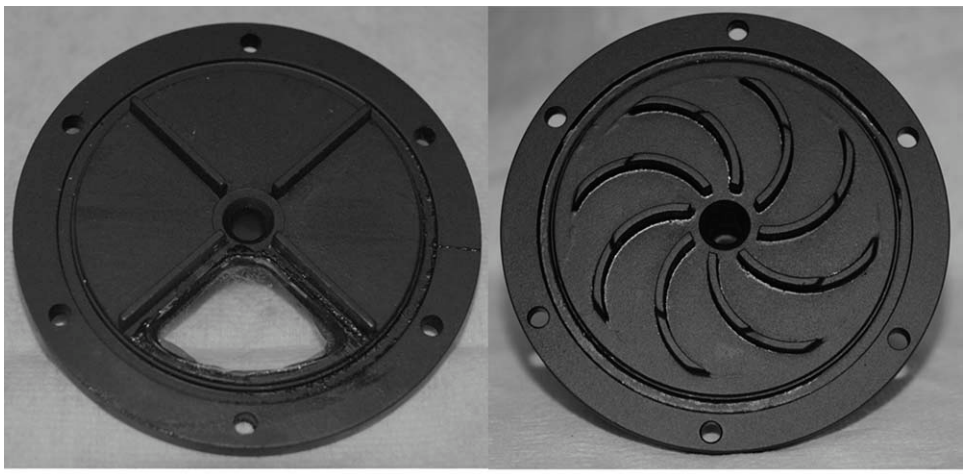


**Figure 3. Snapshots of painted vane plates with (a) four straight vanes, and (b) curved vanes.**

The eight straight vane plate is shown attached in Figure 2.

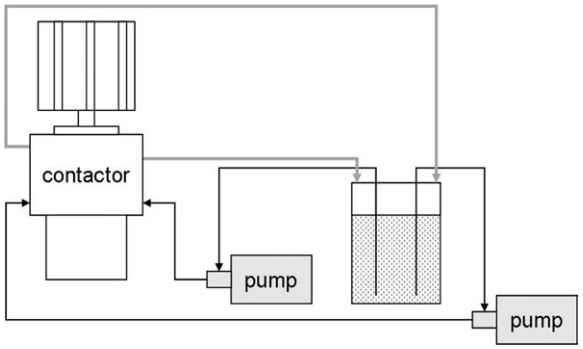


**Figure 4. Flow diagram of the continuous recirculation setup that was used during all experimental measurements.**

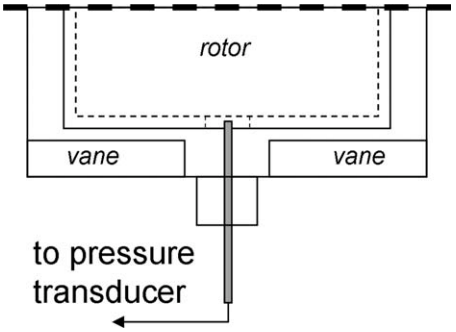


**Figure 5. Diagram of the lower portion of the contactor showing the location of the pressure probe.**

measurements at the same calibrated setting would only be ~1 Pa. At each set of conditions (flow rate and rotor speed) the pressure reading was manually recorded at a rate of ~1 Hz over a typical period of 30 s (N ≈ 30). From these measurements a time average and standard deviation were obtained for each set of conditions.

Pressure measurements were made for each of the three different vane configurations (4-vane, 8-vane, and curved) as a function of rotor speed at a constant flow rate (600 mL/min), and as a function of flow rate for a constant rotor speed (3,600 RPM). The main purpose of these measurements was to aid in selection of an accurate approximation for the pressure at the rotor inlet boundary for input into the mixing zone simulations.[9] One method for approximating the pressure at this point is to assume it is simply equal to the pressure generated by the rotating air column within the separating zone (see Figure 1), and can be calculated according to the Bernoulli equation for rotating flow

$$P_1 - P_2 = \frac{\rho\Omega^2}{2}(r_1^2 - r_2^2) - \rho\mathbf{g}(h_1 - h_2) \tag{3}$$

in which $\rho$ is the mass density of air, $\Omega$ is the rotational speed of the rotor, and $\mathbf{g}$ is the acceleration due to gravity. Taking point 1 (subscript 1 in Eq. 3) as the light-phase rotor outlet ($r = r_{org} = 3.15$ cm), which is open to atmosphere ($P_1 = 0$ Pa), the pressure at the center point of the the rotor inlet $P_2$ (the position of the pressure measurements), can be calculated as a function of the rotor rotation rate (points 1 and 2 are labeled in Figure 1). For example, at 3,600 RPM (377 rad/s) the pressure is calculated to be slightly negative at −83.3 Pa. These measurements were needed to determine if the Bernoulli equation gives an adequate estimate of the pressure at this boundary for input into simulations.

### *High-speed video imaging*

High-speed imaging of the flow in the contactor was performed to provide qualitative observation of the dynamics of the flow in the contactor mixing zone, as well as some quantitative observation of the annular liquid height. High-speed video (using a Redlake MotionPro HS-3-M4 camera) was taken for flow rates of 360, 600, and 830 mL/min at imaging speeds of 100 Hz and 1,000 Hz for each of the three vane configurations (4-vane, 8-vane, curved).

### *Laser doppler velocimetry (LDV)*

The LDV setup was described previously in Wardle et al. 2008,[12] and consisted of a two-component measuring system. Because of the contactor's annular geometry, only backscatter measurements were possible, and, therefore, a transceiver was used rather than an off-axis or forward scatter receiver. The scattering media for the LDV measurements were the entrained air bubbles. Although bubbles are generally not ideal flow tracers,[13] due to the configuration of the centrifugal contactor they are unavoidable. Without using advanced techniques such as laser induced florescence (LIF) for wavelength discrimination, the light scattered from these bubbles would drown out any seed particles. Therefore, no attempt at phase discrimination was made for this study and the LDV measurements were made without the addition of any seeding materials aside from the bubbles. It was assumed that the slip velocity is small, and, therefore, the measured bubble velocity is representative of the bulk flow. Indeed, from repeated measurements using water with 25 mg/L sodium dodecylsulfate (SDS) it was found that while a significant decrease in the bubble size was observed, the LDV measurements changed only very slightly and were, thus, not strongly dependent on the overall air bubble size.[12]

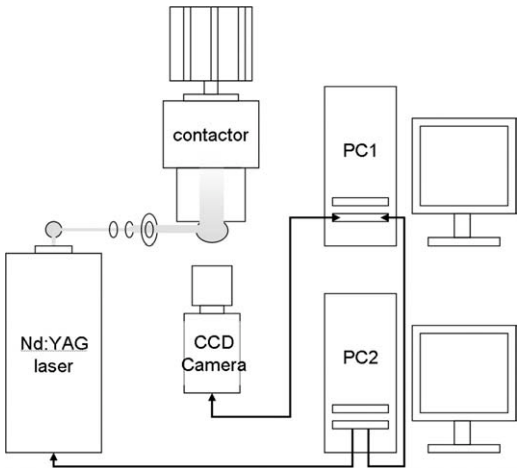


**Figure 6. Diagram of setup for PIV measurements.**

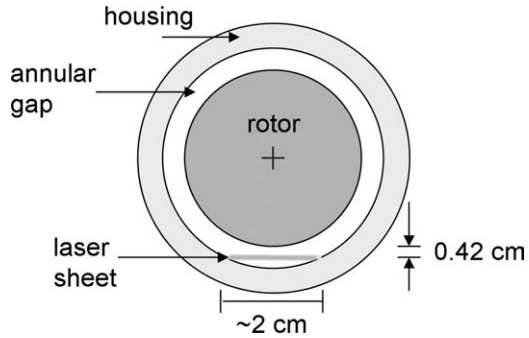


**Figure 7. Sketch showing the orientation of the laser sheet for PIV measurements within the annular region.**

### *Particle image velocimetry (PIV)*

A LaVision particle image velocimetry system was used for 2-D PIV measurements of the flow field both in the annulus of the contactor and underneath the rotor using a Flowsizer3 (model 3S3D) camera. The LaVision DaVis 6.2 software[14] was used for both image acquisition and image processing to obtain mean velocity field information. A double pulsing Nd:YAG laser (532 nm wavelength, $\approx$10 ns pulse width), and the necessary optics were used to generate a thin laser sheet. Firing of the laser and triggering of the camera was done with a LabView program running on a separate computer from the DaVis software which was used to collect the images. A diagram of the PIV system configuration is shown in Figure 6. The physical time delay between the successive laser pulses (and consequently the PIV exposures) was measured using a photodiode monitored with an oscilloscope, and was found to be 154 $\mu$s. For measurements of the flow in the annulus, the laser sheet was directed with a mirror below the contactor up through the window in the vane plate and into the annular gap, such that the laser sheet was vertical and tangential to the rotor at a radial distance of 2.96 cm (0.42 cm from the rotor). At this position the laser sheet was approximately 2 cm wide within the annular region and had a thickness of approximately 250 $\mu$m. Figure 7 shows a sketch depicting the orientation of the laser sheet within the annular region as viewed from above. The PIV measurements in the annulus were not corrected for the curvature of the housing cylinder, and, therefore, only the data on the centerline (where curvature is not an issue) is reported in detail here. For observations of flow under the rotor, the laser sheet was positioned horizontally and directed through the quartz housing wall at a height near the middle of the vanes.

The data acquisition rate for the PIV system was approximately 1 Hz. Due to the low data rate this technique was primarily used for obtaining a spatial map of the mean flow although root-mean square (RMS) velocity values are also reported here. Data were obtained for flow in the annular region of the 4-vane geometry at flow rates of 300, 600, and 1,000 mL/min. For the 600 mL/min flow rate, data were recorded for varying rotor speeds of 314, 377, and 419 rad/s (3,000, 3,600, and 4,000 RPM). For most of the conditions 50 double-frame images were recorded except for runs at 600 mL/min or 3,600 RPM for which 75–100 images were recorded. Regardless, it was observed that the average flow field was not substantially altered for averages of greater than 50 images. Images were processed by cross-correlation using an adaptive multigrid averaging scheme. Two passes of a 64 $\times$ 64 pixel window (with 50% overlap) followed by one pass of a 32 $\times$ 32 pixel window were used.

For flow underneath the rotor on the horizontal laser sheet at the vane mid-height, images were taken at each combination of three flow rate settings (300, 600, and 1,000 mL/min), and three rotor speed settings (3,000, 3,600, and 4,000 RPM) for a total of nine different conditions. These measurements were performed for both of the vane plates with windows (4-vane and 8-vane). It was possible to perform PIV processing of these images; however, due to the large average bubble size in this region this was useful mainly to look at general flow patterns for the various conditions and PIV image processing was performed only for the base conditions (600 mL/min and 3,600 RPM) to give a qualitative description of the flow under the rotor.

As with the LDV measurements, the light scattering media for the PIV were the entrained air bubbles in the flow. Although an exploration of bubble-size effects similar to that described before in relation to the LDV was not made for the PIV measurements, a comparison between LDV- and PIV-measured mean velocities was included previously (see Figure 9 in Ref. 12), and it was found that there is reasonably good consistency between the two except for underneath the rotor where the bubble sizes are large and the PIV measured velocities were seen to be somewhat lower than the LDV measured values.

## Results and Discussion

### *Pressure measurements*

For the overall contactor simulation effort, accurate specification of the boundary between the two regions, particularly the outlet of the mixing zone model, is critical. In

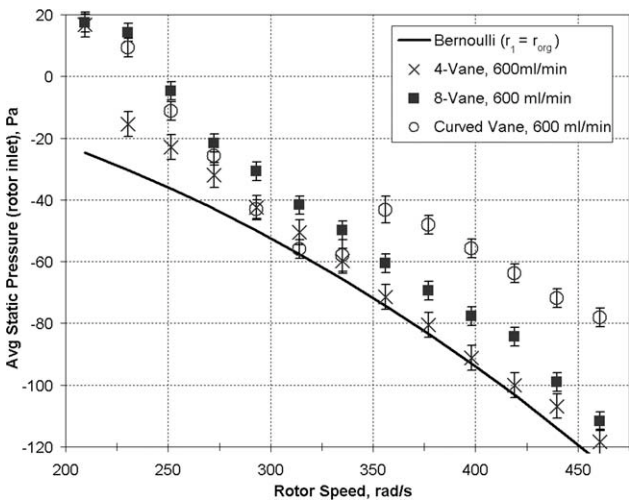


**Figure 8. Measured rotor inlet pressure as a function of rotor speed for the three different vane geometries.**

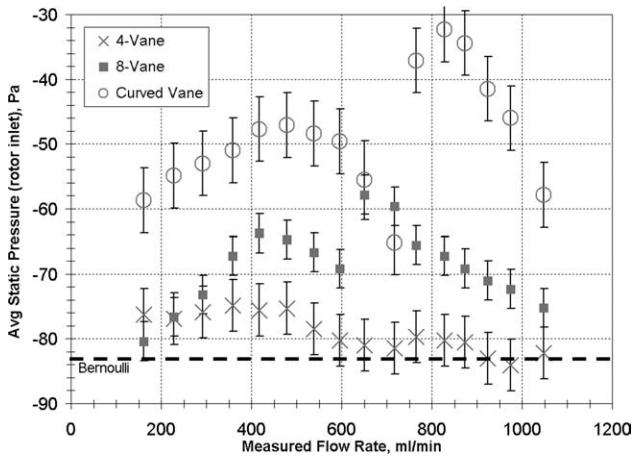


**Figure 9. Measured rotor inlet pressure as a function of flow rate for the three different vane geometries.**

Rotor speed is 377 rad/s (3,600 RPM).

general, it had been previously assumed that the pressure at the rotor inlet is primarily governed by the flow in the rotor—that is, the flow is *pulled* into the rotor by a negative pressure rather than *pushed* in by the force of the flow on the vanes. As simulations proceeded, the validity of this assumption became somewhat unclear, and, therefore, physical measurements of the pressure at the rotor inlet were conducted to provide some insight into the characteristics of this region and aid in the boundary value specification.

The measured pressure as a function of rotor speed is shown in Figure 8 along with the Bernoulli equation (Eq. 3). For the 4-vane geometry, there is good general agreement with the Bernoulli equation, and, thus, it appears that the flow is indeed predominately "pulled" into the rotor by the negative pressure of the rotating column of air in the rotor. For the other vane configurations, however, there are varying degrees of positive deviation from the pressure predicted by Eq. 3. Consequently, it appears that there is also some degree of forcing of the flow into the rotor by the vanes which elevates the pressure relative to that predicted by the Bernoulli equation. Moreover, it was observed that abrupt changes in the annular liquid height were accompanied by changes in the measured pressure. This can be seen in the sudden change in pressure for the curved vanes at approximately 3,400 RPM. Below this speed, there was a sharp decrease in the liquid height as the flow switched abruptly from an "expanded", large void flow to a "collapsed", bubbly flow (this will be discussed more later). (There is also a

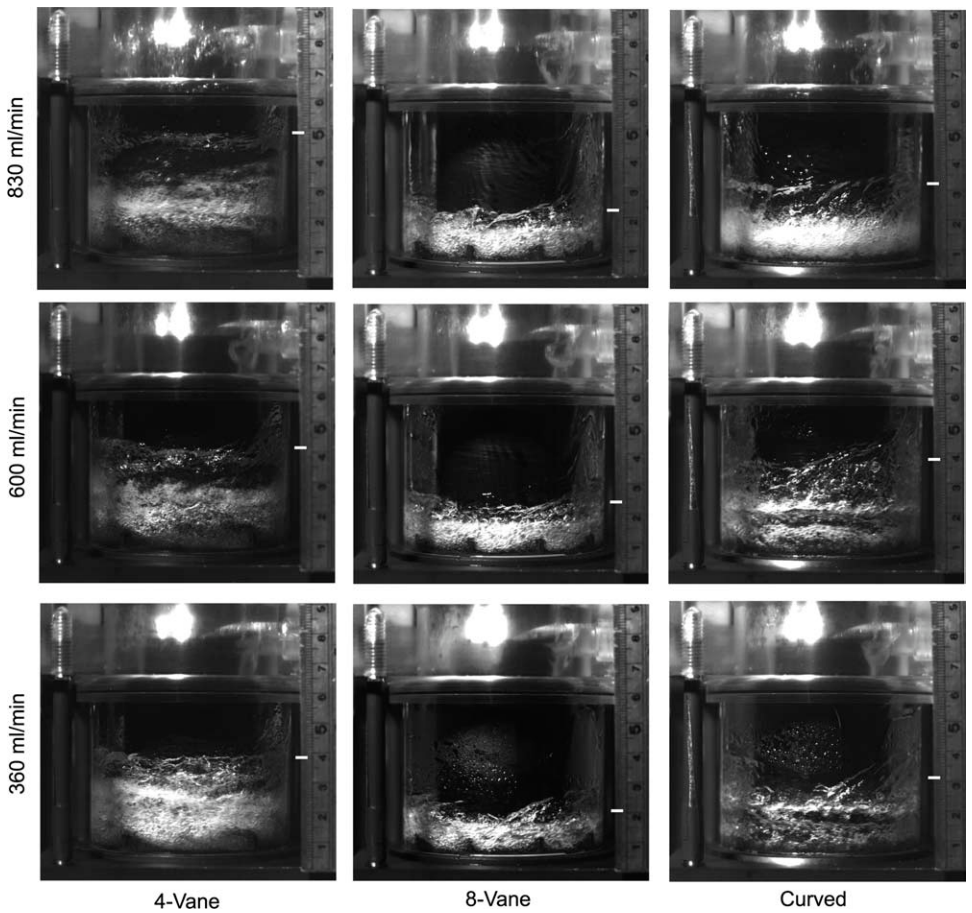


**Figure 10. Snapshots from high-speed imaging (1,000 Hz, 500 $\mu$s exposure) of the flow in the annular region.**

The rotor speed was 377 rad/s (3,600 RPM). The rotor bottom is at approximately 1.3 cm on the ruler

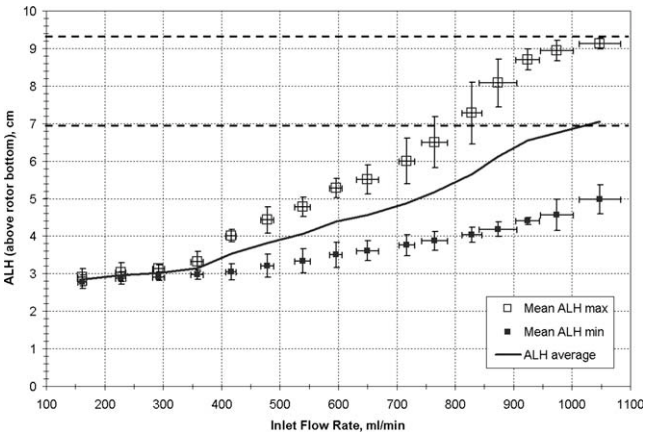


**Figure 11. Annular liquid height observations as a function of flow rate for the 4-vane geometry.**

All flow rates were equally distributed between the two inlets. Error bars denote the standard deviation of a number of repeat observations. The horizontal dashed lines show the position of the bottom of the inlets (7 cm), and the extreme top of the mixing zone (~9.25 cm).

visibly noticeable transition as a function rotor speed for the 8-vane geometry which was observed to occur at approximately 4,000 RPM, although there did not appear to be an obvious effect of this in the pressure data).

Similar behavior can be observed as a function of flow rate (Figure 9). Again, the 4-vane geometry is "well-behaved" relative to the value given by the Eq. 3 (−83.3 Pa). Note also that over the entire range of flow rates for the 4-vane geometry there is a continuous rise in the ALH (and ALH oscillation), but no change in the overall flow pattern (this is described in more detail later, see Figure 11). Such is not the case for either the 8-vane or the curved vane geometries. Both experience a dramatic flow transition as the flow rate goes from high to low (or vice versa). This transition occurs at ≈750 mL/min for the curved vanes as can be seen in pressure measurements shown in Figure 9. The 8-vane geometry also experiences a similar transition, although the transition point was observed to vary over a relatively wide band of possible flow rates (≈350–600 mL/min). Note that the apparent transition for the 8-vane geometry in Figure 9 that occurs at ≈600–650 mL/min was *not* accompanied by an observable flow structure change. For this case, the transition to expanded flow did not occur until about 350 mL/min. The discontinuity observed in the pressure data for this case may have been the result of a change in flow structure under the rotor that was not visually observed but occurs at a higher-flow rate than, and is perhaps a precursor to, the overall transition to expanded flow.

In general, for the "low" end of the flow rate range (below the transition point) the flow in both geometries is an open type flow characterized by a higher ALH, but with large voids within the flow and a distinct "separation line" approximately 0.5 cm above the bottom of the rotor. Above the transition point, the flow collapses down to a more compact flow characterized by a dense bubbly appearance. These "expanded" and "collapsed" flow patterns can be seen for the curved geometry at the 600 mL/min and 830 mL/min settings as shown later in Figure 10. It was also observed, particularly for the 8-vane geometry, that there is a region of operation where the flow pattern becomes unstable and at times even experiences a steady alternation (at ≈1 Hz) between the two flow types for certain flow conditions. It was not possible to determine if there is a liquid volume change between the two flow types; however, it is thought that there is not a change in volume, only a change in overall void distribution. This open (or "expanded") flow structure is described more in the following section.

It is clear that there are effects due to the vane geometry which impact the pressure at the rotor inlet. As intuition might imply, the pressure in this region is indeed somewhat affected by both the flow downstream (in the rotor) and the flow upstream in the vane region under the rotor. Even so, it does appear that the 4-vane case corresponds quite well to the previous assumptions of downstream dominated pressure. These effects for the other vane configurations are not fully understood and more exploration in this area in the future could aid in the development of a rigorous method for specifying the pressure at the rotor inlet for a given rotor speed, flow rate, and geometry. Ultimately, it may be that division of the contactor flow area at this point to facilitate separate simulations of the two contactor regions is not advised for some configurations due to the strong coupling between the inner and outer regions, and a combined modeling approach is needed. However, for the 4-vane geometry this does not appear to be a significant issue as it follows the prediction of

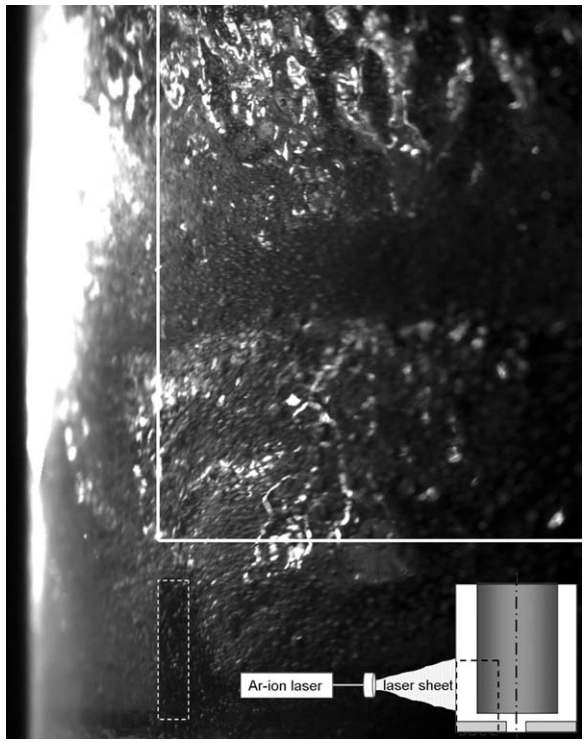


**Figure 12. 10 μs exposed image of the flow in the annular region illuminated by a laser sheet (see inset).**

The approximate location of the rotor and one visible vane are outlined. Flow is from right to left.

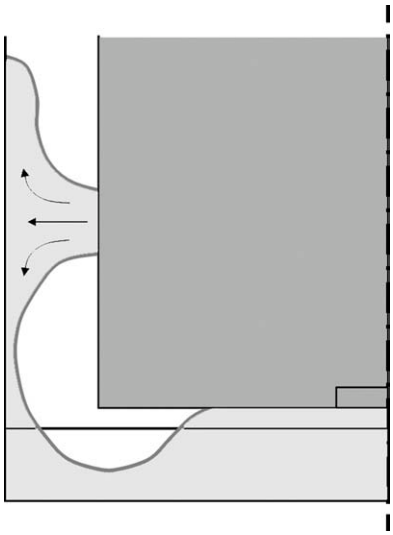

**Figure 13. Simplified sketch of the "expanded" flow structure seen in the 8-vane geometry.**

Similar structure was seen in the curved vane geometry.

the Bernoulli equation quite well and exhibits little flow rate dependence.

### *Flow in annular region*

High-speed imaging of the flow in the annular region was very useful in observing the differences in flow resulting from the different vane designs. Figure 10 shows a composite of snapshots taken from high-speed video imaging of the flow in the mixing zone at several flow rates for each of the three standard geometries. Snapshots were taken at the annular liquid height (ALH) minimum for the 4-vane and curved vane geometries, which both have liquid height oscillations (the curved vane much less so). There are very noticeable differences in annular flow characteristics for the three different vane configurations.

The 4-vane geometry tends to have a significantly higher-liquid level than the others and it was observed that the minimum ALH (as is shown in the figure) for this configuration increases with flow rate. Additional observations of the annular liquid height for this geometry were made over a wide range of flow rates and are plotted in Figure 11. These observations were made by visual estimation of the average maximum and minimum liquid height during operation, and the values reported here are averages over multiple estimations. These visually estimated values are consistent with values obtained from estimation of the ALH in the recorded images. From Figure 11 it is apparent that not only does the minimum ALH increase with increasing flow rate as can be seen in Figure 10, but the ALH oscillation magnitude also increases. It will be shown later that the frequency of this oscillation is inversely proportional to changes in magnitude (i.e., higher frequency for lower magnitude oscillation). Both of these in turn seem to be directly driven by the change in the overall liquid level; an increase in liquid level leads to an increase in oscillation magnitude and a corresponding decrease in frequency.

The 8-vane geometry has a relatively low-liquid level that does not vary significantly with flow rate. This is consistent with observations made previously by others.[6] As noted previously, in the context of the pressure measurements, this geometry also experiences a flow "expansion" at low-flow rates. This transition was found to be somewhat variable, occurring at slightly different flow rate settings on different days. It may have been a function of the contactor unit temperature since it was observed that the expanded flow type (virtually identical in appearance to the flow structure in the curved vane image at 300 mL/min in Figure 10), was steady for flow rates up to $\approx$600 mL/min just after the unit was started up, but occurred only for low-flow rates $\leq$400 mL/min after the unit was warm. As seen in Figure 10, the collapsed flow type was stable down to 360 mL/min during the high-speed imaging of this geometry. This collapsed flow structure had a very low-liquid height ($\approx$1 cm above the rotor bottom) with substantial entrainment of air and a bubbly appearance.

Quite similar to the 8-vane geometry, the curved vane housing also evidences a flow pattern transition which occurs above $\approx$750 mL/min. This transition is indeed apparent for the range of flow rates shown in Figure 10. For the highest flow rate setting (830 mL/min), the flow is similar to the collapsed structure in the 8-vane geometry save that the liquid level is somewhat higher within the curved vane housing. For the two lower flow rate settings, the flow is "expanded" with a relatively stable separation line (evidenced by the cloudy horizontal band) at $\approx$1 cm above the bottom of the rotor. It appears that this band marks the region of highest fluid-rotor contact where the fluid is spun out from the rotor and impinges on the housing wall. Above this band there is a continuous free surface with little contact with the rotor. Below this band there seems to be very intermittent fluid-rotor contact and large voids.

This flow behavior was explored in more detail experimentally with a very limited set of observations of the identical "expanded" flow structure in the 8-vane geometry using a vertically oriented laser sheet. These observations were for settings of 600 mL/min and 3,600 RPM, and during a period when the expanded flow type was stable for these conditions. A snapshot of the annular flow illuminated by the laser sheet is given in Figure 12. The inset shows the orientation of the laser sheet. The bright field in the upper left is generated by light scattering from the high concentration of small bubbles in a ring near the housing wall marking the "separation line" as was seen previously for the curved vane images in Figure 10. As previously described, this image indeed shows a region on the side of the rotor where the liquid appears to be in relatively steady contact with the rotor surface. The authors have chosen to refer to this band as the "separation line" as it appears to demarcate the location of high-fluid-rotor contact and high-relative-radial flow somewhat analogous to that seen in the simplified contactor models[15] and at the "outflow" point of a Taylor-Couette vortex. Above this band, a liquid/air free surface was consistently present for all the laser sheet images taken ($\approx$50), demonstrating the lack of fluid-rotor contact in this region. Below this horizontal band of contact, there were large air voids generated from the intermittent fluid-rotor contact. A cross-section sketch of what this expanded flow structure seems to

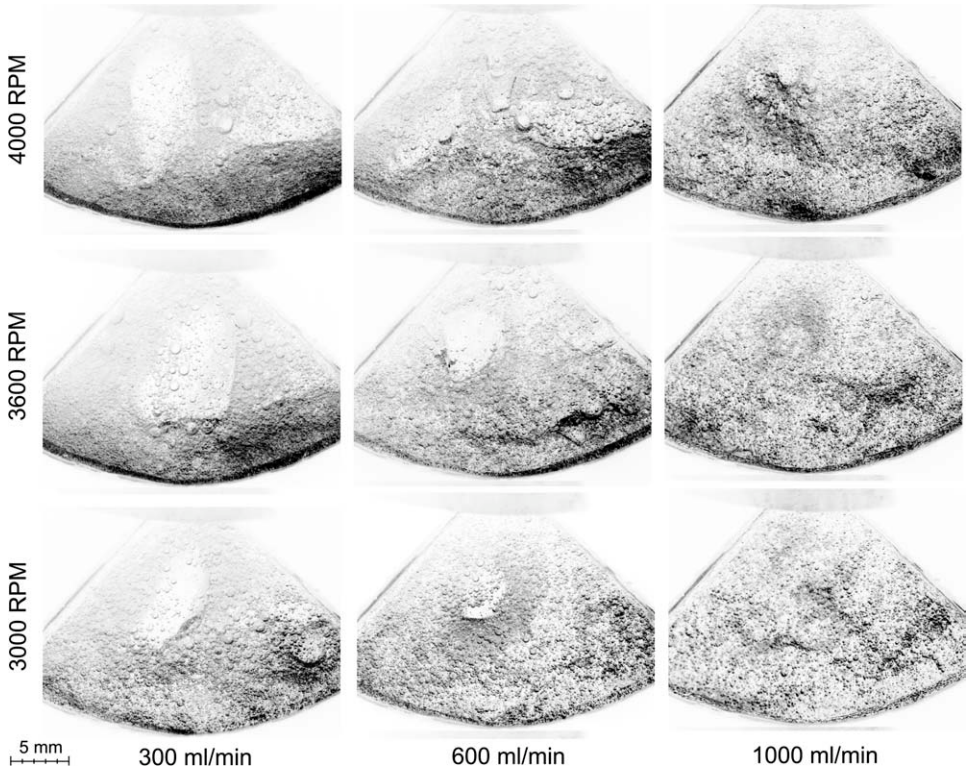


**Figure 14. Flow under the rotor for the 4-vane geometry as a function of flow rate (columns) and rotor speed (rows).**

look like is shown in Figure 13. Although this detailed exploration was for the "expanded" flow structure in the 8-vane geometry, it is likely to be the same for the "expanded" flow structure of the curved vane geometry as seen in the lower two flow rate settings in Figure 10.

### *Flow under the rotor*

For the 4-vane and 8-vane housing geometries, a window was placed in the vane plate to observe the flow in the region between vanes underneath the rotor. The same setup used for particle image velocimetry (PIV) was used for qualitative imaging of the flow in this region. Due to the relatively large bubble sizes, these were not used for quantitative information, but rather simply to observe the general flow patterns. Some PIV-processed flow fields at the standard conditions in the 4-vane and 8-vane geometry are given later in this section. Composite images of the flow under the rotor for each of these geometries at the nine different combinations of three flow rates and three rotor speeds are shown in Figures 14 and 15 for the 4- and 8-vane geometries, respectively. The snapshots shown in the figures were chosen from among the 50–100 images obtained at each setting and are representative of the flow at the given conditions. For both geometries, there is flow rotation in the clockwise direction (see Figure 16 for processed vector fields of the standard conditions).

For the 4-vane geometry (Figure 14), it appears that the effect of flow rate is much more significant than rotor speed for the ranges explored here* as can be seen by the general decrease in bubble size with increasing flow rate. Recall from Figure 11 that the liquid level increases with increasing flow rate. For the lowest flow rate setting, the bubble-size distribution is much larger and there is a relatively stable large bubble that is maintained at the center of a large vortex region (clockwise rotation). It also appeared that the size of this central bubble increased slightly with rotor speed as the rotational speed of this vortex also increased, stabilizing the void. As flow rate is increased, the corresponding increase in liquid level was accompanied by an increase in rotor contact resulting in higher turbulence as evidenced by the shrinking bubble size. The large bubble under the rotor, which was relatively stable for the lowest flow rate, became unstable at higher flow rates and was observed to sporadically be generated, undergo distortion, and then become broken into several smaller bubbles. For the highest flow rate tested (1,000 mL/min), the average bubble size appeared to be quite small ($<250$ $\mu$m); however, in general it appeared that the higher rotor speed was accompanied by larger air pockets near the rotor surface (the underlying "ripples" in these images). Assuming that the air bubble size is directly related to the degree of mixing and turbulence near the rotor, it appears that these images support the general conclusion made previously that there is better mixing for higher liquid levels. This conclusion is further supported by the simulation-based

*Only a narrow range of rotor speeds (3,000–4,000 RPM) was explored because in general the rotor speed is determined by the high degree of phase separation needed within the rotor, and, therefore, low-rotor speeds are typically not used.

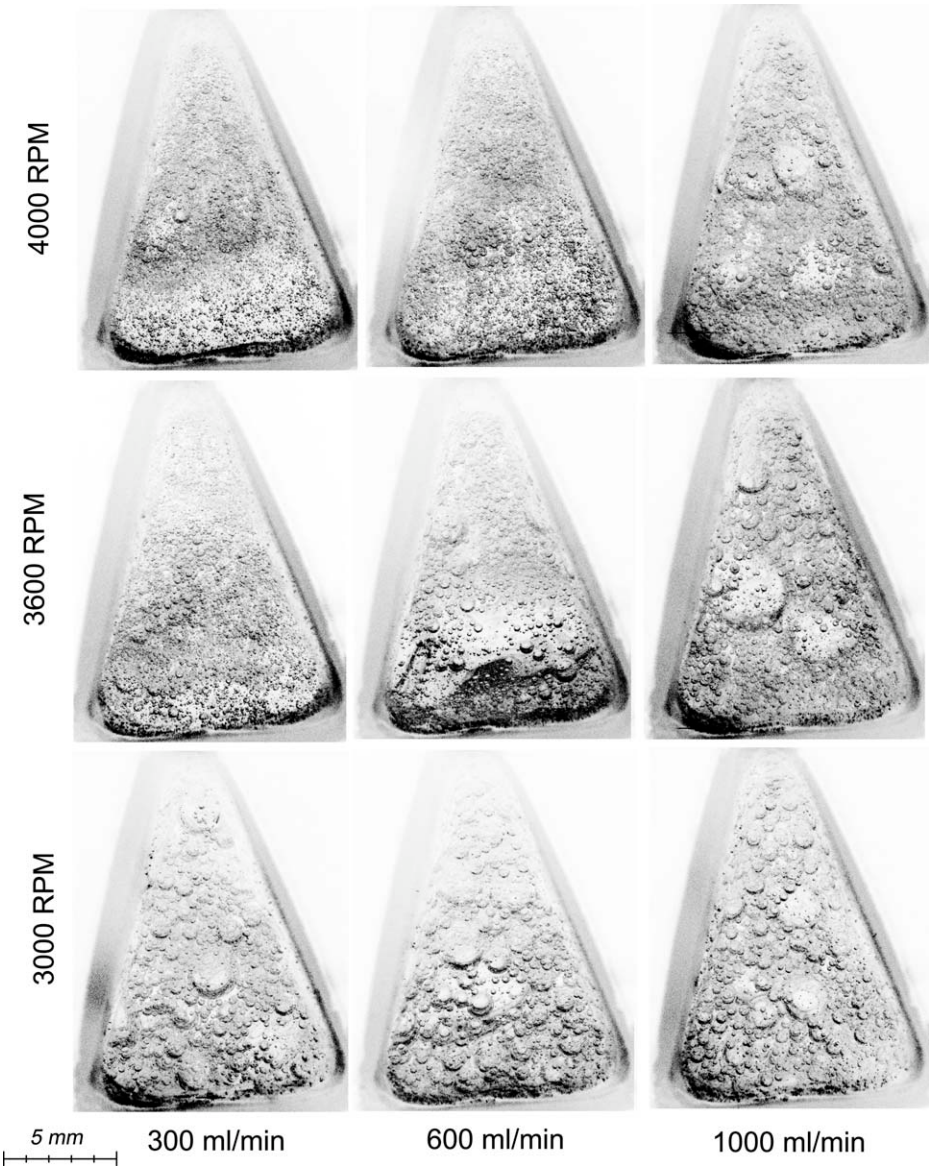


**Figure 15. Flow under the rotor for the 8-vane geometry as a function of flow rate (columns), and rotor speed (rows).**

comparison of turbulence and mixing in contactors presented in a separate article.[9]

For the 8-vane geometry (Figure 15), the combined effect of the rotor speed and flow rate is more complex. In general, it appeared that the type of annular flow structure (expanded or collapsed) which was stable for the given combination of flow rate and rotor speed had the biggest effect on the characteristics of the flow observed under the rotor. For example, the collapsed flow structure was stable for each flow rate condition at the lowest rotor speed setting and the flow is similarly very bubbly for all flow rates with perhaps a slight decrease in average bubble size for the highest flow rate. At the middle rotor speed, the expanded flow structure became stable at the lowest flow rate and the effect on the entrained air bubble size is stark. The same structure was stable for both the low and middle flow rate settings at 4,000 RPM. It was not specifically recorded what type of flow structure was present for the other conditions (mid and high at 3,600 RPM and high at 4,000 RPM), but judging from the appearance of the flow it may have been some unstable combination of the two types.

Although the relatively large bubble sizes in the region under the rotor precluded quantitative use of PIV processed vector fields, these data is still quite informative, for providing a qualitative description of the flow field in this region. The vector field (and corresponding streamlines) for the 4-vane and 8-vane PIV measurements at 600 mL/min and 3,600 RPM are shown in Figure 16. For the 4-vane geometry there is a large central vortex rotating in the clockwise direction (same as rotor rotation) that is shifted slightly off-center in the forward flow direction. The center of this vortex corresponds with the location of the large voids as described in relation to Figure 14. For the 8-vane geometry, there is only a very weak general rotation and the majority of the flow

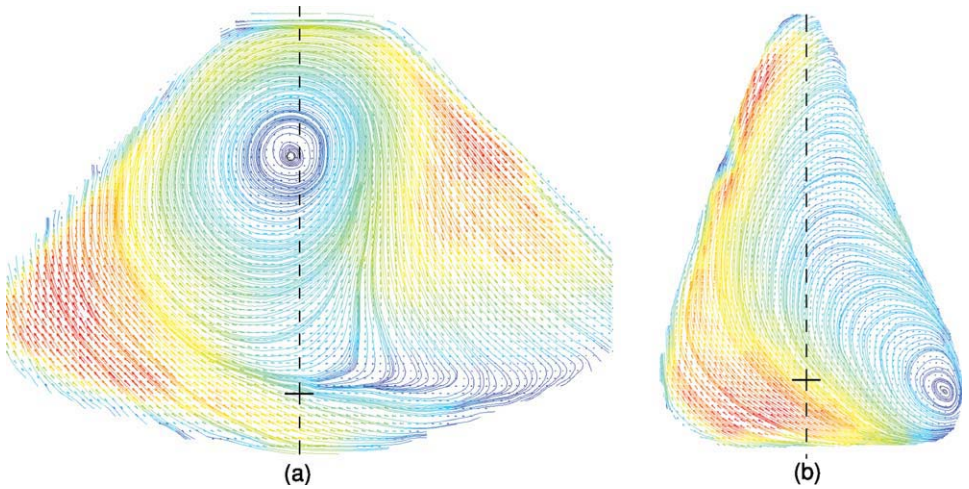


**Figure 16. PIV processed vector fields of the flow underneath the rotor at 600 mL/min and 377 rad/s (3,600 RPM) for the (a) 4-vane and (b) 8-vane geometries.**

Flow rotation is in the clockwise direction. The color scale represents local mean velocity magnitude with the highest values (red) approximately 1 m/s. The approximate location of the outer edge of the rotor is marked on the bisecting line (dashed line). [Color figure can be viewed in the online issue, which is available at www.interscience.wiley.com.]

appears to go radially inward along the forward vane wall toward the axis of the rotor.

### *Velocity measurements*

*Particle image velocimetry (PIV) data.* The time averaged velocity field obtained from PIV analysis of the flow in the annular region is shown (as streamlines) in Figure 17a. The position of the bottom edge of the rotor and the axis of the rotor are delineated on the figure. The vertical extent of the domain shown here is from the bottom of the housing to approximately 1.5 cm above the rotor bottom (same axial extent of data shown in subsequent figures); the width of the domain is approximately 2 cm, but is broadened by the curvature of the cylindrical housing as mentioned previously. The corresponding RMS velocity field is given in Figure 17b. The trailing flow behind one of the housing vanes can be seen in the lower part (below the rotor bottom) of Figure 17a. It is also evident from this figure that there is a distinct average axial height ($\approx$7–8 mm above rotor bottom), below which the flow has a clear downward component and above which the flow has a very slight but noticeable upward component; this upward flow is likely diminished by the steady oscillations of the free surface.[†] This is consistent with the vector fields in the annulus seen in previous CFD simulations.[12] From the velocity fluctuations (Figure 17b), the trailing vortices behind the vane are again evident. The highest measured velocity fluctuations occur near the bottom of the rotor in the region of the plane near the rotor axis—the point where the plane is closest to the rotor. Recall, however, that the laser sheet is somewhat removed from the surface of the rotor and the velocity fluctuations at this distance are significantly less than the levels very near the rotor. Even so, these measurements do support the type of fluid-rotor contact predicted by the simulations of this geometry where there is a band of continuous contact near the bottom of the rotor.[12]

As no correction was applied to account for the curvature of the housing and consequently only the data along the vertical centerline (rotor axis) are quantitatively valid for direct comparison with simulation. Such comparison between the PIV results and simulation predictions for the standard conditions is reported elsewhere.[9]

Quantitative PIV of the flow underneath the rotor was not performed due to the large bubble distribution and bubble-bubble interaction in this region. The general flow patterns observed experimentally in this region were discussed in the previous section and are shown in Figure 16.

## PIV as a Function of Rotor Speed and Flow Rate

PIV data similar to that presented in the previous section for the base-case conditions were also obtained for other flow rates and rotor speed settings as described in the Experimental Methods section. All these data are from the 4-vane geometry. Only the data along the vertical line within the measurement plane that is even with the axis of the rotor are given here (vertical dot-dash line in Figure 17).

The PIV-measured average velocity profiles for three rotor speeds (3,000 RPM, 3,600 RPM, 4000 RPM) are shown in Figure 18. The corresponding RMS velocity profiles are shown in Figure 19. It is apparent from the plots of the mean velocity profiles that with increasing rotor speed the velocity magnitude increases but the overall shape of the profile (i.e., axial location of maximum tangential and axial velocities) does not change significantly. As for the velocity fluctuations, in general a similar sort of behavior is evident although the magnitude of the change appears small.

On the other hand, changes in inlet flow rate result in slightly more complex behavior. The PIV-measured average velocity profiles for various total inlet flow rate settings (300 mL/min, 600 mL/min, 1,000 mL/min) are shown in Figure 20. The corresponding RMS velocity profiles are

[†]The consistency of these PIV measurements was also checked by repeating the measurements with the camera viewing area shifted upward; the axial height of this separation line relative to the rotor bottom was found to be consistent between the two sets of measurements.

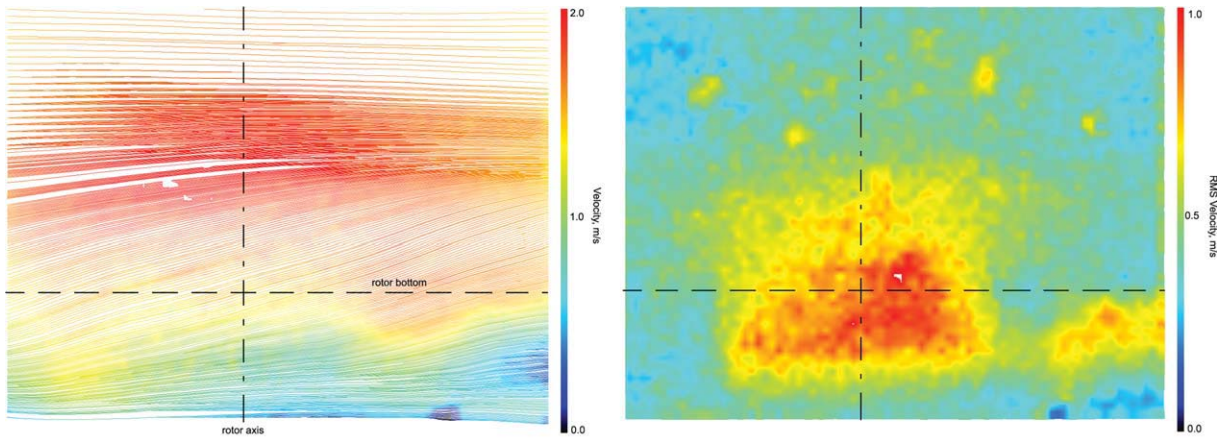


**Figure 17. Plot of (a) streamlines for the time-averaged velocity field and (b) the RMS velocity magnitude distribution interpolated from PIV of flow in the annular region of the 4-vane contactor at 600 mL/min and 377 rad/s (3,600 RPM).**

The flow is from right to left. For reference, the rotor bottom and axis are delineated [Color figure can be viewed in the online issue, which is available at www.interscience.wiley.com.]

shown in Figure 21. Two profiles are shown for the 300 mL/min flow rate setting; one is for 300 mL/min in the front inlet only (same side as PIV plane), and the other, the back inlet only. No measurement was taken with an evenly distributed inlet flow (i.e., 150 mL/min in each inlet) as was the case for both the 600 mL/min and 1,000 mL/min settings. Note that there is an increase in the average annular liquid height (ALH), and ALH oscillation magnitude with increasing flow rate (see Figure 11). For a total inlet flow rate of 300 mL/min the annular liquid height (above the rotor bottom) was observed to be approximately 3 cm with little oscillations; for flow rates above ≈300 mL/min, the ALH oscillation magnitude increases steadily. For 600 mL/min, the minimum ALH is around 3.5 cm and the max 5.3 cm. For 1,000 mL/min, the minimum and maximum ALH are approximately 4.8 cm and 9 cm. The increase in the minimum ALH is directly related to an increase in the liquid holdup in the mixing zone. This effect may partly explain the difference in the tangential velocity profiles for the different flow rates. However, it does not seem to explain the axial velocity profiles. There, the lower flow rate setting actually was found to have higher axial velocity magnitudes.

As was seen with the rotor speed changes, the changes in the RMS velocities (Figure 21) are less dramatic, although there does appear to be a general trend toward increasing velocity fluctuation with increasing flow rate. This is in general

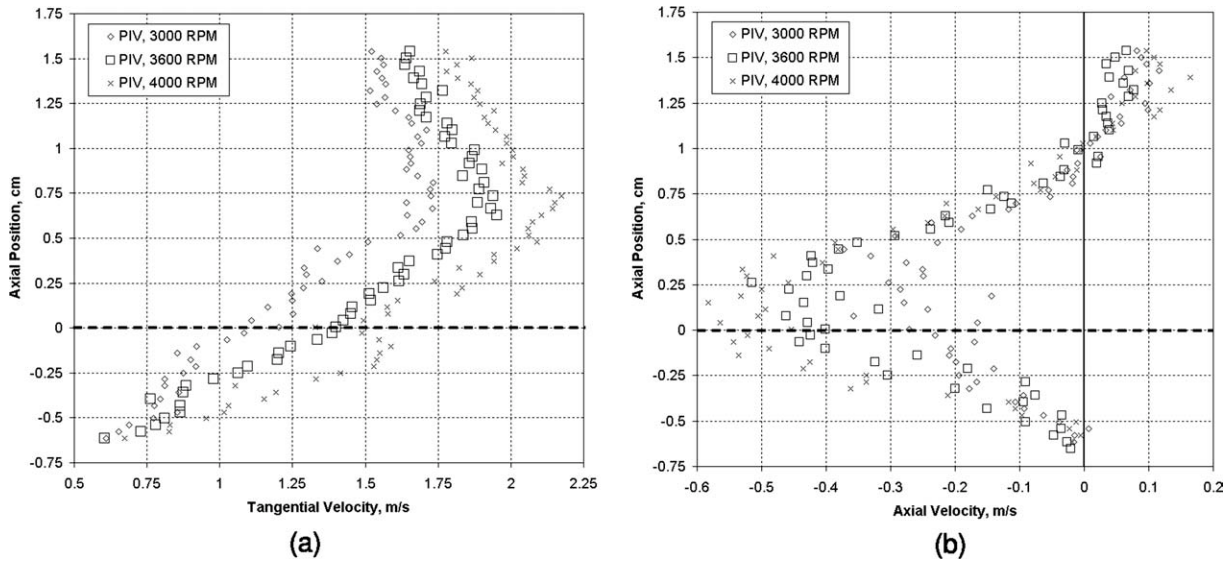


**Figure 18. PIV data of the (a) mean tangential velocity and (b) mean axial velocity along a vertical line even with the rotor axis for rotor speeds of 314 rad/s (3,000 RPM), 377 rad/s (3,600 RPM), and 419 rad/s (4,000 RPM).**

The rotor bottom is noted by the horizontal dashed line

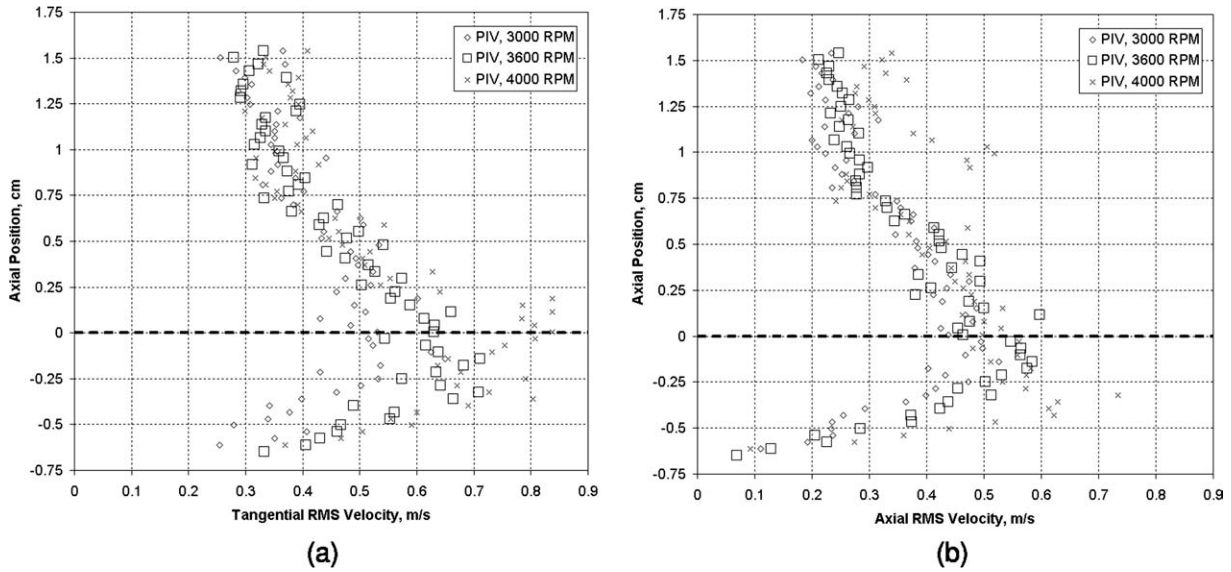


**Figure 19. PIV data of the (a) RMS tangential velocity and (b) RMS axial velocity for the three different rotor speeds.**

agreement with the change in annular liquid height. Greater liquid height results in greater fluid-rotor contact and greater turbulence in the liquid phase.

In general, these data could be better explained by additional CFD simulations to look at the overall flow patterns and complex fluid-rotor interactions as inlet flow rate and rotor speed are varied. Understanding these effects may ultimately aid in the optimization of operation of the centrifugal contactor for a given process flow rate.

### *ALH Oscillation (4-vane) as a function of rotor speed and flow rate*

As previously noted, the 4-vane geometry was characterized by a steady oscillation in the liquid level. The variation in frequency of the liquid height oscillation was observed as a function of rotor speed (from LDV as described in Ref. 12) and inlet flow rate (from high-speed video imaging). In general, it was observed that the oscillation frequency was inversely related to the rotor speed and flow rate—that is, increasing the rotor speed results in a decrease in the oscillation frequency as too does increasing the inlet flow rate. The observed values are shown in Tables 1 and 2. In general, it appears that the change in oscillation frequency can be explained by the relationship between the mixing zone liquid volume (as observed by the minimum ALH) and the fluid—rotor contact—which decreases as liquid volume decreases. For example, this effect seems to explain how the observed oscillation frequency changes with flow rate (Table 1); a lower flow rate results in lower liquid volume, less fluid-

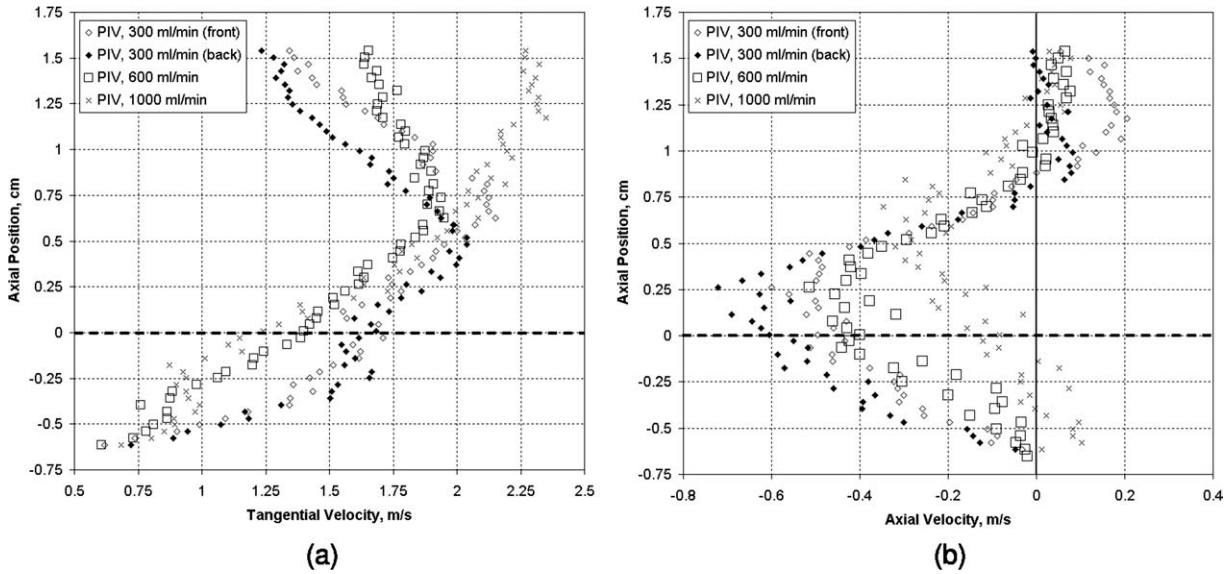


**Figure 20. PIV data of the (a) mean tangential velocity and (b) mean axial velocity along a vertical line even with the rotor axis for total inlet flow rates of 300 mL/min, 600 mL/min, and 1,000 mL/min.**

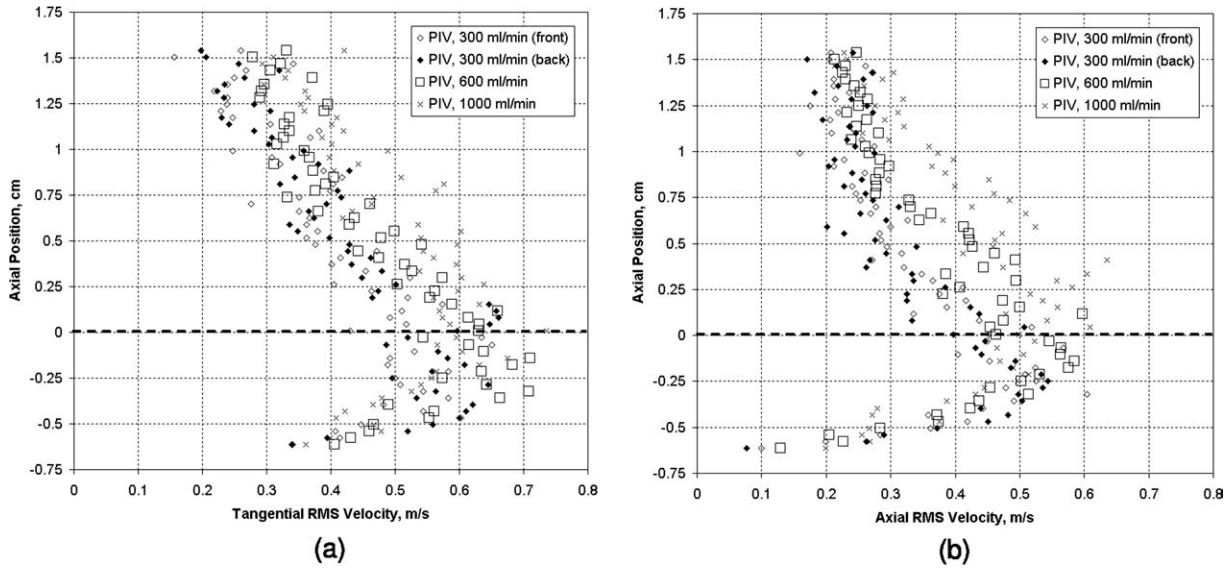


**Figure 21. PIV data for the (a) RMS tangential velocity and (b) RMS axial velocity for various total inlet flow rates.**

rotor contact, and consequently less momentum imparted by the rotor to the fluid, resulting in a lower oscillation magnitude but a higher frequency.

For the effect of varying rotor speed (Table 2), the liquid volume (minimum ALH) was also seen to increase slightly with higher speed for this geometry. Although one might reasonably postulate that for a given liquid height a higher rotor speed would have less fluid-rotor contact, it appears that this is more than compensated for by the greater surface velocity of the rotor, resulting in a larger amount of momentum imparted to the fluid. This momentum of the fluid is translated into potential energy as the fluid is spun out and up the housing wall and then back into kinetic energy as the fluid collapses back down where it contacts the rotor again. This greater magnitude of oscillation results in a lower oscillation frequency. CFD studies for a range of flow conditions might provide greater insight into this effect and the relationship between fluid-rotor contact and liquid height oscillation as a function of rotor speed.

## Conclusions

It is clear from these experiments that the mixing vane configuration has a significant effect on the flow in the mixing zone of the annular centrifugal contactor. The measurements of pressure at the rotor inlet demonstrate the different levels of flow forcing by the different vane geometries as a function of rotor speed and flow rate. Sharp flow transitions in the annular region (i.e., transition from and collapsed to an expanded flow structure in the curved vane configuration) were found to have an effect on the measured pressure. Based only on the 4-vane geometry results, this pressure data was used to develop an adequate method for specification of the outlet boundary condition for the mixing zone simulations.[9] However, it may be possible to use the data from the other configurations to devise a more general method for specifying a model-boundary condition, which accounts for the differences due to vane geometry, rotor speed, and flow rate.

From flow observations of the annular region, the liquid heights (and by extension the liquid volumes) for the three different vane geometries tested here were found to be quite different. The 4-vane geometry had a higher-liquid height than either of the other two configurations for the range of flow rates tested. Although ''mixing'' was not quantitatively evaluated directly from these experiments (e.g., through measurement of the turbulence dissipation rate for the different configurations), companion computational efforts have demonstrated a direct relationship between increased liquid height and increased mixing.[9] Consequently, for low to moderate flow rates, the 4-vane geometry would have greater mixing (and greater fluid residence time). However, at flow

**Table 1. Frequency of Liquid Height Oscillation in 4-vane Geometry as a Function of Flow Rate (constant rotor speed of 3,600 RPM) as Estimated from the High-Speed Video Images**

| Inlet Flow Rate, ml/min | Frequency, Hz | Minimum ALH, cm | Maximum ALH, cm |
|---|---|---|---|
| 360 | 5.41 ± 0.26 | 3.0 | 3.3 |
| 600 | 4.88 ± 0.29 | 3.5 | 5.3 |
| 830 | 4.47 ± 0.17 | 4.0 | 7.3 |

ALH maxima and minima were approximated by direct external observation (see Figure 11).

**Table 2. Frequency of Liquid Height Oscillation in 4-vane Geometry as a Function of Rotor Speed (Constant Flow Rate of 600 mL/min) as Measured with LDV**

| Rotor Speed, RPM | Frequency, Hz | Minimum ALH, cm | Maximum ALH, cm |
|---|---|---|---|
| 3000 | 5.21 ± 0.07 | 3.1 | 4.4 |
| 3600 | 4.75 ± 0.16 | 3.5 | 5.3 |
| 4000 | 4.55 ± 0.05 | 3.8 | 7.0 |

ALH maxima and minima are average values approximated from direct external observation.

rates above ≈1 L/min the maximum liquid excursions in this geometry reach the top of the mixing zone. Thus, the use of the 4-vane geometry would likely be limited to total inlet flow rates below 1 L/min to avoid the possibility of phase contamination into the lower collector ring.

For flow under the rotor, the difference in mixing between the 4-vane and 8-vane geometries for different rotor speeds and flow rates was inferred by qualitative observation of the air bubble sizes in this region. Consistent with the observations of flow in the annular region, it was seen that the 4-vane geometry tended to have much smaller air bubbles than the 8-vane configuration. For the 8-vane configuration, the type of flow structure (collapsed or expanded) in the annular region had a clear effect on the characteristics of the flow under the rotor.

Simulations reported elsewhere have been performed for the base-case conditions (600 mL/min and 3,600 RPM) and the comparison with these experiments was found to be quite good.[9,12] It is anticipated that the additional data presented here could be useful for further validation of contactor simulations at different flow conditions. In particular, the quantitative PIV and LDV data at different flow rates and rotor speeds in the 4-vane geometry could be useful for comparison with CFD simulations for a range of flow conditions.

## Acknowledgments

This research was performed under appointment to the U.S. Dept. of Energy Nuclear Engineering and Health Physics Fellowship Program sponsored by the U.S. Department of Energy's Office of Nuclear Energy, Science, and Technology.

## Literature Cited

1. Drain F, Vinoche R, Duhamet J. 40 years of experience with liquid-liquid extraction equipment in the nuclear industry. In: *Waste Management Symposium, WM'03*. Tuscon, AZ; February 23–27, 2003.
2. Vandegrift GF, Regalbuto MC, Aase S, Bakel A, Battisti TJ, Bowers D, Byrnes JP, Clark MA, Emery JW, Falkenberg JR, Gelis AV, Pereira C, Hafenrichter L, Tsai Y, Quigley K, Vander Pol MH. Designing and demonstration of the UREX+ process using spent nuclear fuel. The International Conference on Advances for Future Nuclear Fuel Cycles, ATATLANTE; June 21–24, 2004; Nimes, France.
3. Bernstein G, Grosvenor D, Lenc J, Levitz N. Development and performance of a high-speed annular centrifugal contactor. Technical Report ANL-7969, Argonne National Laboratory, 1973.
4. Bernstein G, Grosvenor D, Lenc J, Levitz N. A high-capacity annular centrifugal contactor. *Nucl Technol*. 1973;20:200–202.
5. Birdwell JF, Anderson KK. Evaluation of mass transfer performance for caustic-side solvent extraction of cesium in a convenional 5-cm centrifugal contactor. Technical Report ORNL/TM-2001/278, Oak Ridge National Laboratory, 2002.
6. Leonard R, Regalbuto M, Aase S, Arafat H, Falkenberg J. Hydraulic performance of a 5-cm contactor for caustic-side solvent extraction. Technical Report ANL-02/18, Argonne National Laboratory; 2002.
7. Law J, Tillotson R, Todd T. Evaluation of the hydraulic performance and mass transfer efficiency of the CSSX process with the optimized solvent in a single stage of 5.5-cm diameter centrifugal contactor. Technical Report INEEL/EXT-02–01106, Idaho National Engineering and Environmental Laboratory, 2002.
8. Wardle KE. *Computational and Experimental Analysis of the Flow in an Annular Centrifugal Contactor*. Madison, WI: University of Wisconsin-Madison; 2008. Ph.D. dissertation.
9. Wardle KE, Allen TR, Anderson MH, Swaney RE. Analysis of the effect of mixing vane geometry on the flow in an annular centrifugal contactor. *AICHE J*. 2009;55:2244–2259.
10. Andereck CD, Lui S, Swinney HL. Turbulent flow between concentric rotating cylinders at large Reynolds number. *J Fluid Mech*. 1986;164:155–183.
11. Wardle KE, Allen TR, Swaney RE. CFD simulation of the separation zone of an annular centrifugal contactor. *Sep Sci Technol*. 2009;44:517–542.
12. Wardle KE, Allen TR, Anderson MH, Swaney RE. Free surface flow in the mixing zone of an annular centrifugal contactor. *AIChE J*. 2008;54:74–85.
13. Mei R. Velocity fidelity of flow tracer particles. *Exp Fluids*. 1996; 22:1–13.
14. Lavision GmbH. *FlowMaster Manual for DaVis 6.2*. 2002.
15. Wardle KE, Allen TR, Swaney R. CFD study of the flow in an annular centrifugal contactor. *Sep Sci Technol*. 2006;41:2225–2244.

*Manuscript received July 3, 2008, revision received Mar. 3, 2009, and final revision received Oct. 8, 2009.*